Research Article

Core−Shell Nanofibrous Materials with High Particulate Matter Removal Efficiencies and Thermally Triggered Flame Retardant Properties

Kai Liu,[†,‡] Chong Liu,[†,‡] Po-Chun Hsu,[†] Jinwei Xu,[†] Biao Kong,[†] Tong Wu,[†] Rufan Zhang,[†] Guangmin Zhou,[†] William Huang,[†] Jie Sun,[†] and Yi Cui*[,†,§]

[†]Department of Materials Science and Engineering, Stanford University, Stanford, California 94305, United States
[§]Stanford Institute for Materials and Energy Sciences, SLAC National Accelerator Laboratory, 2575 Sand Hill Road, Menlo Park, California 94025, United States

Ⓢ *Supporting Information*

ABSTRACT: Dust filtration is a crucial process for industrial waste gas treatment. Great efforts have been devoted to improve the performance of dust filtration filters both in industrial and fundamental research. Conventional air-filtering materials are limited by three key issues: (1) Low filtration efficiency, especially for particulate matter (PM) below 1 μm; (2) large air pressure drops across the filter, which require a high energy input to overcome; and (3) safety hazards such as dust explosions and fires. Here, we have developed a "smart" multifunctional material which can capture PM with high efficiency and an extremely low pressure drop, while possessing a flame retardant design. This multifunctionality is achieved through a core−shell nanofiber design with the polar polymer Nylon-6 as the shell and the flame retardant triphenyl phosphate (TPP) as the core. At 80% optical transmittance, the multifunctional materials showed capture efficiency of 99.00% for $PM_{2.5}$ and >99.50% for $PM_{10-2.5}$, with a pressure drop of only 0.25 kPa (0.2% of atmospheric pressure) at a flow rate of 0.5 m s^{-1}. Moreover, during direct ignition tests, the multifunctional materials showed extraordinary flame retardation; the self-extinguishing time of the filtrate-contaminated filter is nearly instantaneous (0 s/g) compared to 150 s/g for unmodified Nylon-6.
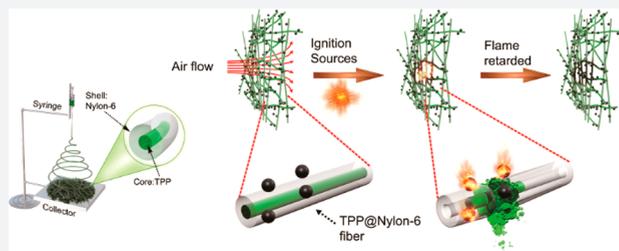
$\mathbf{D}$ust filtration is crucial for minimizing air pollutant emissions in industrial processes, with conventional air-filtering devices, e.g., baghouses, seeing wide deployment in industries such as power generation, chemical production, and agricultural processing.[1−3] However, current dust filtration systems remain limited by the following challenges: (1) Commonly used devices such as baghouses use wovens composed of micrometer-sized fibers for filtration and thus have low filtration efficiencies (<95%) and perform especially poorly for particulate matter (PM) below 1 μm,[1,2] which contributes significantly to the serious PM air pollution seen in developing countries.[4−7] (2) Conventional methods are energy intensive; thick filters and low void space result in a large pressure drop over the filter which must be overcome.[1,3,8] A bag filter for the filtration of 100 000 m^3 waste gas requires roughly 36 kWh of energy to operate, not accounting for the energy required to compress air.[9] In 2010 alone, the energy cost for industrial gas waste filtration was estimated to be as high as ∼20 TWh just in China.[10] (3) Dust filtration materials are vulnerable to fires and explosions.[11−16] This is particularly important considering that more than 70% of dust processed in industry is combustible.[15,16] Combustive dusts accumulated on the dust filters are readily ignited by sources such as open

flames or electrostatic discharge; fires then propagate from the filter to suspended dust clouds, causing dust explosions.[15] Catastrophic accidents related to dust explosions are reported every year;[11−16] from 1980 to 2005, at least 281 industrial dust fires and explosions occurred in the United States, which caused at least 119 fatalities and 718 injuries.[14]

Here, by fabricating nanofibers with a core−shell structure, we have developed a multifunctional material that not only achieves a high filtration efficiency for PM_{10} (particulate matter smaller than 10 μm) and $PM_{2.5}$ (particulate matter smaller than 2.5 μm) with a low air pressure drop, but also significantly suppresses fire hazards. As shown in Figure 1, the nanofibers with a core−shell structure were fabricated by electrospinning. Nylon-6 is used as the polymer shell, and triphenyl phosphate (TPP), a widely employed organophosphorus-based flame retardant, is used as the core (TPP@Nylon-6). There are several aspects that make the design novel and efficient: (1) the Nylon-6 polymer shell efficiently captures PM because of its large dipole moment (3.6 D for the repeating unit),[17] ensuring strong binding between the fiber surface and polar
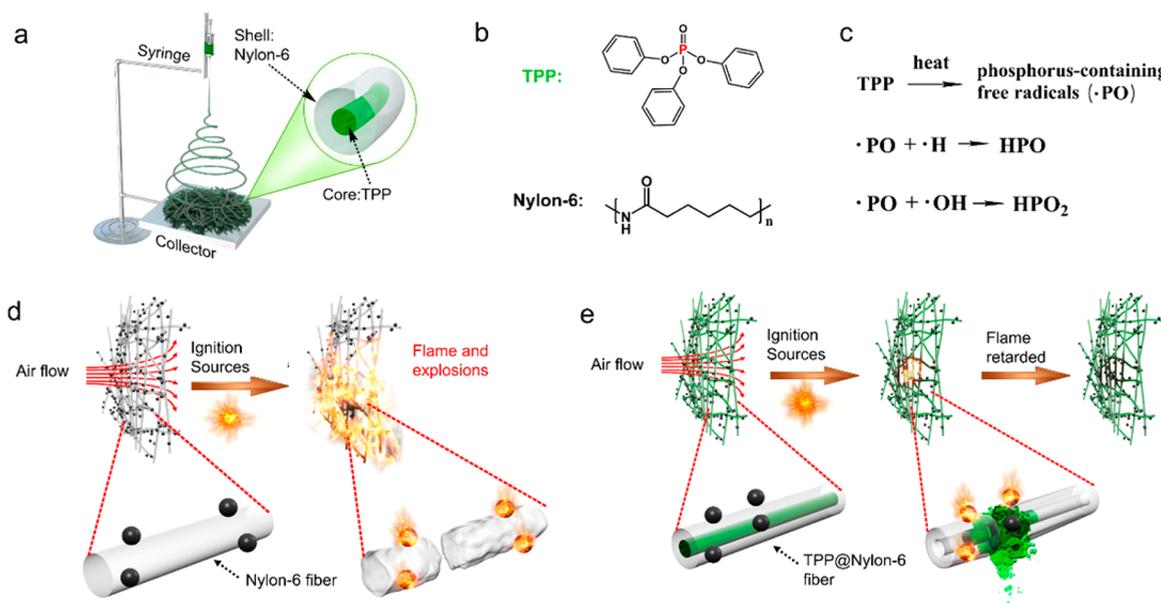
Figure 1. Schematic showing the multifunctional air filter. (a) Schematic illustration for the fabrication of the nanofibers by electrospinning. The air filtration material is composed of nanofibers with a core−shell structure, where Nylon-6 is used as the polymer shell and TPP is the core. (b) Molecular structure of TPP and Nylon-6. (c) The TPP exhibits flame retardancy by scavenging ·H and·OH free radicals during combustion. (d) The air filtration material composed of Nylon-6 nanofibers. Combustive dusts accumulated on the filter are easily ignited by ignition sources, which can cause dust explosions. (e) The working mechanism of the TPP@Nylon-6 smart air filtration material. In normal conditions, the Nylon-6 shell efficiently captures PM. During combustion of the flammable filtrate, the Nylon-6 shell is melted and the TPP flame retardant core of the fiber diffuses out and suppresses the fire.

PM particles.[8] Moreover, hydrogen bonds on surface Nylon-6 molecules result in strong interfiber bonding within the nanofiber network and outstanding mechanical strength of the air filtration material. (2) In a combustion event, the flame retardant core, TPP, diffuses through the melted Nylon-6 shell and extinguishes fires by scavenging ·H and·OH free radicals generated during combustion (Figure 1c).[18] (3) The TPP flame retardant located at the core of the fiber does not impact filtration efficiencies of the filter. These features result in highly effective, multifunctional dust filtration materials that mitigate fire and explosion risk through a nanoengineered "fire extinguisher".

To fabricate the desired TPP@Nylon-6 fiber, TPP and Nylon-6 were dissolved in formic acid with a 1:3 weight ratio of TPP/Nylon-6. The solution was placed into a syringe and directly used for electrospinning. Nanofibers were successfully obtained, as indicated by the scanning electron microscope (SEM) image shown in Figure 2a. Thermogravimetric analysis (TGA) analysis was employed to give quantitative information about the composition of the nanofiber. As shown in Figure 2b, for TPP@Nylon-6, there was substantial weight loss starting at a temperature of approximately 200 °C and ending at approximately 320 °C, indicating loss of TPP from the core−shell nanofiber. For comparison, pure TPP was also heated under the same conditions, as shown by the red dash line in Figure 2b. The weight loss started at ∼200 °C and ended at ∼260 °C. Upon heating, the escape of TPP from the Nylon-6 composite nanofiber occurred over a wider temperature range compared with that of the pure TPP, indicating that TPP diffusion and evaporation is kinetically impeded by the Nylon-6 polymer shell. Further heating led to a second gravimetric loss due to evaporation of Nylon-6 at ∼400 °C for TPP@Nylon-6, which is consistent with the TGA curve of pure Nylon-6 (black dotted line in Figure 2b). In total, the first
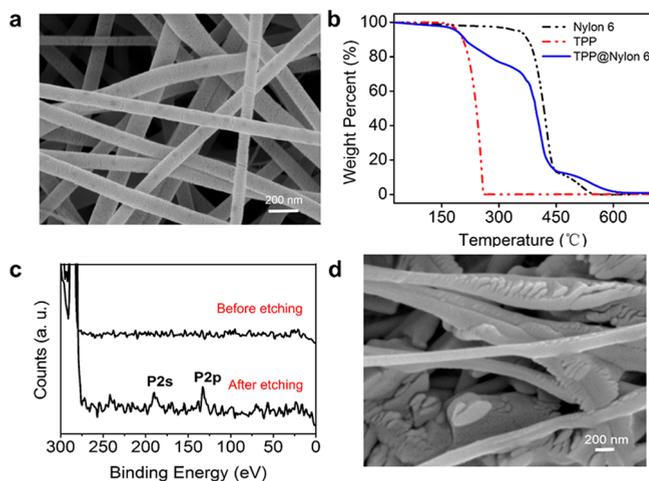

Figure 2. Characterization of the TPP@Nylon-6 nanofibers. (a) SEM images of the pristine nanofibers. (b) TGA curves of Nylon-6 (black dotted line), TPP (red dotted line), TPP@Nylon-6 nanofibers (blue curve). (c) XPS characterization on the pristine TPP@Nylon-6 nanofibers before and after etching. (d) SEM of the nanofibers after etching.

and second gravimetric losses account for approximately 25% and 75% of the total sample weight, respectively. This suggests that the weight ratio of TPP/Nylon-6 in the microfiber is 1:4, which is similar to the starting 1:3 weight ratio of TPP and Nylon-6 in the electrospinning solution.

X-ray photoelectron spectroscopy (XPS) was employed to further probe the core−shell structure of the nanofibers. As shown in Figure S1, strong peaks corresponding to N and C were detected, indicating the presence of Nylon-6 on the surface of the fibers. No peaks corresponding to P were observed (Figure 2c), indicating negligible TPP on the fiber

surface. Ion etching of the fiber surface allows the interior composition to be probed; after etching for 30 s, P 1s and P 2p peaks were detected (Figure 2c), while the intensity of the N peak decreased (Figure S1). This confirms that the nanofiber structure consists of a TPP core encapsulated within a Nylon-6 shell. The inner structure was exposed after etching and is shown in the SEM image in Figure 2d. TPP molecules are prone to form stacks of flake-like crystals (Figure S2), which can be observed clearly in Figure 2d. Moreover, there is a thin polymer layer coating these nanoflakes, which acts as a shell protecting the flakes. We attribute the formation of the electrospun TPP@Nylon-6 core–shell structure to the following: (1) The solubility difference between Nylon-6 and TPP in the solvent, in which TPP shows much higher solubility compared with Nylon-6. As the solvent evaporates during electrospinning, Nylon-6 precipitates earlier than TPP, forming the shell of the nanofiber, while the TPP remains soluble in the remnant solvent and deposits inside the Nylon-6 shell as the solvent evaporates. (2) In the Taylor cone during electrospinning, the strong divergence of the electric field induces migration of highly polar Nylon-6 polymer chains toward the liquid/air interface, leading to a core–shell structure.[19,20]

The nanofibers were synthesized through electrospinning onto a rough copper foil collector and then peeled off from the foil and transferred to a mesh substrate. As illustrated in Figure S3, the transfer of electrospun nanofibers is performed as follows: (1) Electrospinning of the nanofibers onto the rough surface of commercial copper foil. The rough surface minimizes the contact between the nanofiber and the substrate surface, which is important for the later transfer. (2) The air filtration material framework is laminated onto the copper foil, sandwiching the nanofiber layer between the framework and the copper substrate. (3) The framework is then peeled off from the copper foil, with nanofibers remaining bonded to the framework due to stronger adhesion. The Nylon-6 shell of the nanofiber exhibits strong fiber–fiber bonding due to hydrogen bonds between fibers, resulting in a neat transfer of the fiber network to the filter framework.

Following the successful transfer of the nanofiber film, we fabricated air filtration materials at different optical transmittances (corresponding to different thickness) to test their filtration performance. The PM was generated by burning incense, which produces a PM yield greater than 45 mg g^{-1} burned. This smoke contains a variety of pollutant gases, including CO, CO$_2$, NO$_2$, SO$_2$, and volatile organic compounds such as benzene, toluene, xylenes, aldehydes, and polycyclic aromatic hydrocarbons,[21] acting as a model system with many of the components present in polluted air. As shown in Figure 3a,b, SEM was used to characterize the air filtration material before and after filtration. Prior to filtration, the fibers are isotropic along the fiber axis, but as polluted air passes through the filter, PM particles are captured and bound to the fiber surface. To approximate the efficiency of PM particle removal, we fabricated air filtration materials with varying optical transmittances by controlling the electrospinning time and then calculated the removal efficiencies by measuring the PM count in air before and after passing through the filter. As indicated by Figure 3c,d, the filters exhibited excellent capture efficiencies for both PM$_{2.5}$ and PM$_{10-2.5}$ over a wide range of optical transmittance levels. The efficiency for PM$_{2.5}$ capture was 99.00% at ∼80% transmittance, which increased to >99.9% at transmittances lower
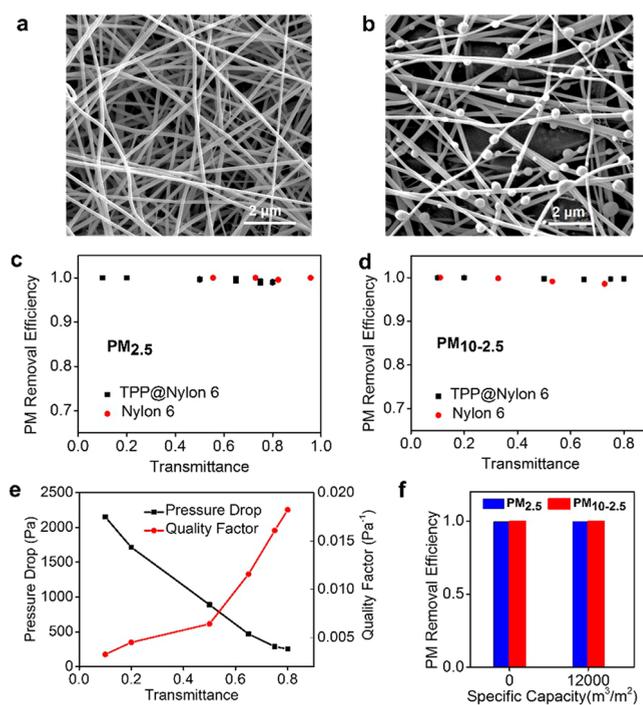

Figure 3. The TPP@Nylon-6 air filtration material shows good PM filtration performances. SEM images of the filter (a) before and (b) after PM filtration. (c) PM$_{2.5}$ removal efficiencies of the TPP@Nylon-6 filters at different transmittances. (d) PM$_{10-2.5}$ removal efficiencies of the TPP@Nylon-6 filters at different transmittances. Flame retardant TPP@Nylon-6 filters are compared against Nylon-6 filters. (e) Pressure drop and quality factor of air filtration materials at different filter transmittances. (f) PM$_{2.5}$ and PM$_{10-2.5}$ removal efficiencies of air filtration materials at different specific capacities.

than 50% (Figure 3c). For PM$_{10-2.5}$ particles, the efficiency was >99.50% at all transmittances as shown in Figure 3d. The filtration efficiencies for pure Nylon-6 nanofibers are similar to TPP@Nylon-6 nanofibers due to identical surface properties, showing that incorporation of flame retardant in the nanofibers does not compromise PM filtration efficiencies.

Maintaining significant air flow is an important performance parameter for a viable air filtration material; to evaluate the practical performance of our flame retardant TPP@Nylon-6 filter, we measured the air pressure drop (ΔP) across the device at different optical transmittances. The change in air pressure across the air filtration material is shown in Figure S4. For a face velocity of 0.5 m s^{-1}, at 80% optical transmittance, the pressure drop was only 250 Pa, or 0.2% of atmospheric pressure. Considering that ΔP increases with filter thickness and decreases with transmittance, quality factor (QF; Table S1) is employed to comprehensively evaluate the overall performance of the air filtration material. QF considers both efficiency and pressure drop, and is defined as QF = $-\ln(1 - E)/\Delta P$, where E is PM removal efficiency and ΔP is the pressure drop of the filters. Generally, the higher the QF, the better the filter. As seen in Table S1, the TPP@Nylon-6 air filtration material we fabricated shows much higher QF than commercial filters, especially at high transmittances. The PM capture capacity of the flame retardant air filtration material was evaluated at 75% transmittance, with a PM$_{2.5}$ concentration of 4300 μg m^{-3}. As shown in Figure 3f, even when the specific purification capacity, i.e., the volume of the purified air divided by the area of the filter, reaches as high as 12 000 m^3/

m^2, the TPP@Nylon-6 filter still maintained a high $PM_{2.5}$ and $PM_{10-2.5}$ removal efficiency of 99.8%. For practical applications, the lifetime of the transparent filter with the transmittance of 75% is expected to be above ~520 h under the hazardous PM level (PM index 150). After this long-term filtration, filtrate particles captured on the filter were aggregated into large particle domains, as shown through SEM in Figure S5. Despite the high capture efficiency, significant void space remains uncovered, indicating high purification capacity of the transparent air filtration materials.

The core–shell structure of the TPP@Nylon-6 fibers not only results in high PM filtration efficiency, but also grants excellent flame retardancy. The thermal response of the TPP@Nylon-6 filters was first studied by differential scanning calorimetry (DSC); as shown in Figure 4a, there are two
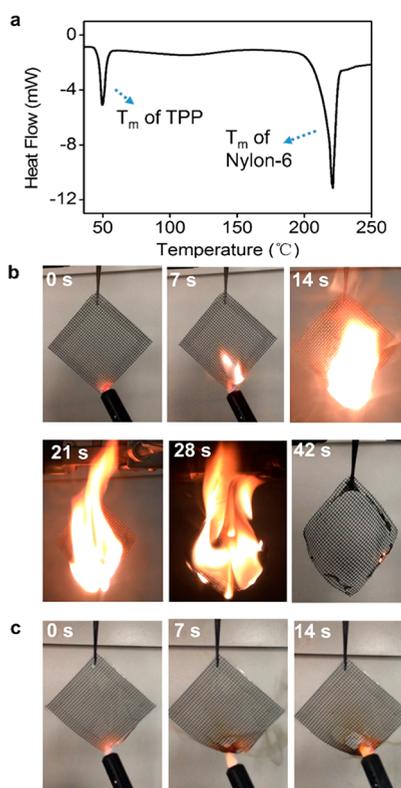

Figure 4. Flame retardancy of the TPP@Nylon-6 air filtration material. (a) DSC curve of the TPP@Nylon-6 air filtration material. Vertical flame testing of the air filtration materials fabricated with (b) Nylon-6 and (c) TPP@Nylon-6 nanofibers. In (b) and (c), the filters were wetted by vegetable oil, which is used as a model system for combustible filtrates. These filters were exposed to a direct flame of a lighter until they were ignited, after which the flame was removed.

endothermic peaks located at ~50 °C and ~220 °C, corresponding to the melting points of TPP and Nylon-6 respectively (Figure S6). As the temperature of the filtrate-saturated air filtration material increases toward the combustion temperature, the flame retardant TPP is melted and later released when the Nylon-6 shell melts. To demonstrate flame retardancy, filters were wetted by vegetable oil, which we use as a model system for combustible filtrates, and then subjected to vertical flame testing. These filters were exposed to a direct flame until they were ignited, after which the flame was removed. As shown in Figure 4b, upon exposure to direct flame for 7 s, the Nylon-6 nanofiber filters ignited, and the

flame quickly spread. The Nylon-6 flame was vigorous and bright, until the whole filter burned to completion. The self-extinguishing time (SET), which was obtained by normalizing the flame combustion time against the oil mass, was calculated to be ~150 s/g. In contrast, the flame on the TPP@Nylon-6 filters quickly self-extinguished after ignition (Supporting Video). As shown in Figure 4c, even after 14 s of exposure to a direct flame, the TPP@Nylon-6 nanofiber filter remained intact, which is in great contrast to the situation of Nylon-6 filter. Thus, the SET is nearly 0 for the TPP@Nylon-6 filters, indicating that the TPP in the core of the TPP@Nylon-6 fibers gave the air filtration material excellent flame retardancy.

In conclusion, we have fabricated a "smart" multifunctional material which not only efficiently captures PM, but also exhibits flame retardancy upon thermal triggering, which is highly important for safe operation with combustible filtrates. During normal function, the highly polar Nylon-6 shell enables the materials to effectively capture PM with low pressure drop across the filter. For filters fabricated at 80% optical transmittance, the PM capture efficiency was 99.00% for $PM_{2.5}$ and >99.50% for $PM_{10-2.5}$, with an air pressure drop of only 250 Pa (only 0.2% of atmospheric pressure). In the event of fire, the flame retardant TPP core is released as the Nylon-6 shell melts, extinguishing the fire nearly instantaneously. This is reflected in the self-extinguishing time, which is nearly 0 s/g for the TPP@Nylon-6, compared to 150 s/g for Nylon-6 alone. The core–shell nanostructure enables the multi-functionality of this smart filter, allowing excellent filtration performance and flame retardancy without compromise of either parameter. We anticipate further extension of core–shell nanoengineered structures for multifunctional materials in broad and novel applications.

■ ASSOCIATED CONTENT

Ⓢ Supporting Information

The Supporting Information is available free of charge on the ACS Publications website at DOI: 10.1021/acscents-ci.8b00285.

> Additional characterizations including XPS character-ization, digital photo of the TPP reagents, schematics illustrating the film transfer process, schematic showing the setup for air pressure measurement, performance summary table, SEM of the TPP@Nylon-6, DSC of TPP and Nylon-6 (PDF)
> Supporting videos (AVI1, AVI2)

■ AUTHOR INFORMATION

Corresponding Author

*E-mail: yicui@stanford.edu.

ORCID Ⓞ

Kai Liu: 0000-0003-3362-180X

Rufan Zhang: 0000-0003-1774-0550

Guangmin Zhou: 0000-0002-3629-5686

Yi Cui: 0000-0002-6103-6352

Author Contributions

‡K.L. and C.L. contributed equally to this work. K.L., C.L., and Y.C. conceived and designed the experiments. A.G. and L.F. made the figures. K.L., C.L., and Y.C. wrote the manuscript. All authors helped do the experiments and discussed the results and commented on the manuscript.

Notes

No unexpected or unusually high safety hazards were encountered.

The authors declare no competing financial interest.

■ REFERENCES

(1) Cora, G. C.; Hung, Y. T. Controlling industrial particulate emissions: a practical overview of baghouse technology. *Environ. Qual. Manage.* **2002**, *11*, 53.

(2) Hinds, W. C. *Aerosol Technology: Properties, Behavior, and Measurement of Airborne Particles*; John Wiley & Sons: New York, 1998.

(3) Saleem, M.; Krammer, G. Effect of filtration velocity and dust concentration on cake formation and filter operation in a pilot scale jet pulsed bag filter. *J. Hazard. Mater.* **2007**, *144*, 677.

(4) Dominici, F.; Greenstone, M.; Sunstein, C. R. Particulate matter matters. *Science* **2014**, *344*, 257.

(5) Seinfeld, J. H. Urban Air Pollution: State of the Science. *Science* **1989**, *243*, 745.

(6) Betha, R.; Behera, S. N.; Balasubramanian, R. Southeast Asian Smoke haze: fractionation of particulate-bound elements and associated health risk. *Environ. Sci. Technol.* **2014**, *48*, 4327.

(7) Khalid, B.; Bai, X. P.; Wei, H. H.; Huang, Y.; Wu, H.; Cui, Y. Direct blow-spinning of nanofibers on a window screen for highly efficient PM2.5 removal. *Nano Lett.* **2017**, *17*, 1140.

(8) Liu, C.; Hsu, P. C.; Lee, H. W.; Ye, M.; Zheng, G. Y.; Liu, N.; Li, W.; Cui, Y. Transparent air filter for high-efficiency $PM_{2.5}$ capture. *Nat. Commun.* **2015**, *6*, 6205.

(9) The importance of effective dust removal. *Tissue World Magazine*, January/February 2014; http://www.tissueworldmagazine.com/latest-headlines/the-importance-of-effective-dust-removal/, date of accession: April 5, 2018.

(10) Data source: The volume of industrial gas waste emission in China, https://d.qianzhan.com/xdata/details/a4d0ce6d9cc24ce3.html, date of accession: April 5, 2018.

(11) Eckhoff, R. K. *Dust Explosions in the Process Industries: Identification, Assessment and Control of Dust Hazards*, 3rd ed.; Gulf Professional Publishing, Elsevier: Boston, 2003.

(12) Cashdollar, K. L. Overview of dust explosibility characteristics. *J. Loss Prev. Process Ind.* **2000**, *13*, 183.

(13) Joseph, G. CSB Hazard Investigation Team. Combustible dusts: A serious industrial hazard. *J. Hazard. Mater.* **2007**, *142*, 589.

(14) Blair, A. S. Dust explosion incidents and regulations in the United States. *J. Loss Prev. Process Ind.* **2007**, *20*, 523.

(15) Abbasi, T.; Abbasi, S. A. Dust explosions—Cases, causes, consequences, and control. *J. Hazard. Mater.* **2007**, *140*, 7.

(16) Vijayaraghavan, G. Review article: Dust explosions — a major industrial hazard. *Inter. J. Adv. Eng. Tech II* **2011**, 83.

(17) Xu, J.; Liu, C.; Hsu, P. C.; Liu, K.; Zhang, R. F.; Liu, Y. Y.; Cui, Y. Roll-to-roll transfer of electrospun nanofiber film for high efficiency transparent air filter. *Nano Lett.* **2016**, *16*, 1270.

(18) Laoutid, F.; Bonnaud, L.; Alexandre, M.; Lopez-Cuesta, J.-M.; Dubois, Ph New prospects in flame retardant polymer materials: From fundamentals to nanocomposites. *Mater. Sci. Eng., R* **2009**, *63*, 100.

(19) Mu, X. Y.; Liu, Y.; Fang, D. W.; Wang, Z. L.; Nie, J.; Ma, G. P. Electric field induced phase separation on electrospinning polyelectrolyte based core—shell nanofibers. *Carbohydr. Polym.* **2012**, *90*, 1582.

(20) Liu, K.; Liu, W.; Qiu, Y. C.; Kong, B.; Sun, Y. M.; Chen, Z.; Zhuo, D.; Lin, D. C.; Cui, Y. Electrospun core-shell microfiber separator with thermal-triggered flame-retardant properties for lithium-ion batteries. *Sci. Adv.* **2017**, *3*, e1601978.

(21) Lin, T.-C.; Krishnaswamy, G.; Chi, D. S. Incense smoke: clinical, structural and molecular effects on airway disease. *Clin. Mol. Allergy* **2008**, *6*, 3.